HHS Public Access

Author manuscript

Angew Chem Int Ed Engl. Author manuscript; available in PMC 2021 December 01.

Published in final edited form as:

Angew Chem Int Ed Engl. 2020 November 02; 59(45): 19894–19898. doi:10.1002/anie.202008416.

Salivary excretion of renal clearable silver nanoparticles

Shaoheng Tang[#], **Yingyu Huang**[#], **Jie Zheng**[*]

Department of Chemistry, The University of Texas at Dallas, 800 W. Campbell Rd., Richardson, TX 75080 (USA)

[#] These authors contributed equally to this work.

Abstract

Salivary elimination is an important pathway for the body to excrete small molecules, digestive enzymes. However, very few engineered nanoparticles can be excreted through salivary glands, which often host bacteria or viruses during infection and involve in disease transmission. Herein, we reported a new finding that renal clearable glutathione coated AgNPs (GS-AgNPs) can selectively accumulate in the submandibular salivary gland, followed by being excreted in its excretory duct. By conducting head-to-head comparison on in vivo transport and interactions of both GS-AgNPs and glutathione coated gold nanoparticles (GS-AuNPs) with the same sizes, we found that low-density GS-AgNPs showed much higher vascular permeability than GS-AuNPs and can rapidly penetrate into submandibular salivary glands, be efficiently taken up by striated and excretory duct cells and eventually secreted into saliva. Since many nanoparticles exhibit potent broad-spectrum antimicrobe and antiviral activities, this finding indicates a new potential of nanomedicines in the infectious disease treatment.

Graphical Abstract

[*] **Corresponding Author** jiezheng@utdallas.edu .

The authors declare no competing financial interest.

Supporting information for this article is given via a link at the end of the document.

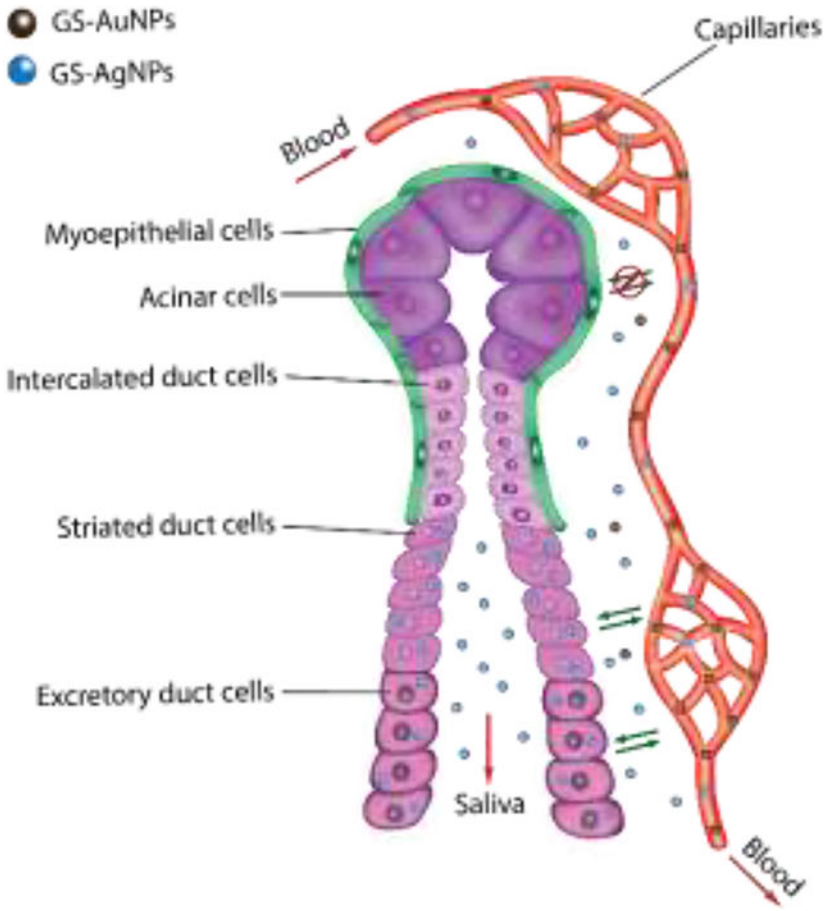

Salivary excretion: a new way to go for engineered nanoparticles

Keywords

Submandibular salivary glands; Silver nanoparticles; Gold nanoparticles; Fluorescence imaging

Nearly 1–2 liters of saliva is produced by human salivary glands every day[1]. As one of three major salivary glands[1], the submandibular salivary gland (**SSG**) is responsible for generating 65–70% saliva in the oral cavity via acinus cells.[2] SSG is composed of acinar cells, different types of duct cells and myoepithelial cells enveloped by blood capillaries (Scheme 1).[3] The SSGs actively interact with the plasma components due to the exchange of blood-derived molecules into the saliva-producing acinus cells. As a result, saliva contains digestive enzymes that can break down starch into simpler sugars[4] as well as secretory IgA, and lysozymes with antimicrobial and antiviral functions.[5] On the other hand, salivary glands are also known to host and excrete bacteria and viruses[6] as well as involve in infectious disease transmission[7]. However, very few studies have been dedicated to investigating nanoparticle transport and interactions in the salivary glands even though many of them are known to exhibit potent antibacterial and antiviral functions.[8]

Renal clearable engineered nanoparticles are known to rapidly distribute in the entire body after intravenous injection.[9] In the meantime, they can behave like small molecules to be rapidly eliminated out of the body through the kidneys and have minimized accumulation in the background tissues if no interactions occur.[10] As a result, they not only can reach different organs in a short period of time but also be very sensitive to local nano-bio interactions.[11]

For example, by specifically designing the structures of renal-clearable organic dyes, Choi et.al. achieved selective targeting of the NIR-emitting organic dyes to bone and thyroid gland through phosphonation and halogenation, respectively, which demonstrated great applications for bioimaging and disease prognosis.[12] In addition, by investigating the size-dependency of the glomerular filtration using a series of well-defined gold nanoclusters (AuNCs), we revealed that ultrasmall AuNCs with size in the sub-nanometre regime specifically interacted with the glomerular endothelial glycocalyx in the kidneys.[13] Moreover, we found that the density of renal-clearable metal nanoparticles can significantly impact their *in vivo* transport kinetics as well.[14] Although extensive studies have been done to understand their transport and interactions in the kidneys, very little attention has been focused on other excretion pathways such as salivary elimination even though they also play many important physiological functions.

Herein, we reported our latest finding that renal clearable NIR-emitting glutathione coated silver nanoparticles (GS-AgNPs) can selectively accumulate in the submandibular salivary glands and light up the glands within the first three hours after intravenous injection, followed by excretion into saliva. On the other hand, no similar transport and clearance in the submandibular salivary glands were observed from GS-AuNPs with the same size and surface chemistry. Further studies on the pharmacokinetics and biodistributions at the different injection time points indicated that the origin of selective accumulation of GS-AgNPs in SSG is because GS-AgNPs have much higher vascular permeability than GS-AuNPs due to their lower density. In the meantime, efficient uptake of the striated and excretory duct cells further enhanced the retention of GS-AgNPs, resulting in their longer retention in the SSG than GS-AuNPs. Moreover, excretion of GS-AgNPs from the duct cells into saliva was also observed. Taken together, these findings first report the high permeable engineered nanoparticles that can be efficiently transported to SSG and be taken up by and excreted through striated and excretory duct cells. Since both saliva and silver nanoparticles are well known for their antibacterial function, introducing silver nanoparticles that can be secreted through the salivary glands might enhance antibacterial and antiviral function of saliva through this unique bio-nano hybridization method and treat infectious diseases.

GS-AuNPs and GS-AgNPs were synthesized according to our previously described thermal reduction method.[14–15] Briefly, a fresh aqueous solution of reduced glutathione was added into aqueous solutions of $HAuCl_4$ or $AgNO_3$ under stirring. Then the mixtures were heated at 95°C and stirred for 0.5h and 37h, respectively. Transmission electron microscopy (TEM) and dynamic light scattering (DLS) were used to determine their core size and hydrodynamic diameters (HD). As illustrated in Figure 1, these two NPs have almost identical morphology, core sizes (~2.6 nm, Figure 1c and Figure S1) and HD (~3.1 nm, Figure 1c and Figure S1). To compare the surface chemistry of these two NPs, FT-IR

spectrums were obtained with the purified dry samples of GS-AuNPs and GS-AgNPs (Figure 1d). The presence of the C=O stretch at around 1700 cm^{-1} and the disappearance of the S-H stretch at 2525 cm^{-1} indicated the successful coating of GSH on the particle surface via the formation of Au-S and Ag-S band. Due to the ligand-to-metal charge transfer in ultrasmall metal nanoparticles, both GS-AuNPs and GS-AgNPs exhibited strong near-infrared (NIR) emissions with a maximum at 810 and 710 nm, respectively (Figure 1e).[10] Since protein corona can dramatically increase the size of ultrasmall NPs, which can essentially affects NPs' in vivo fate, we tested the serum protein binding of GS-AuNPs and GS-AgNPs by incubating them with bovine serum albumin (BSA) at pH 7.4 for 30 min and determined their binding affinities towards BSA using agarose gel electrophoresis. As shown in Figure 1f, the BSA protein bands stained by Coomassie Brilliant Blue 250 (CBB250) were well- separated from the yellow bands of Au and Ag NPs, indicating no obvious protein binding for both nanoparticles. Both nanoparticles showed higher mobility than BSA due to the presence of highly negative glutathione molecules on nanoparticle surface while GS-AuNPs exhibited almost identical electrophoretic mobility compared with that of GS-AgNPs, further suggesting that these two NPs possess the same surface chemistry, size but just different densities.

By taking advantages of the strong intrinsic NIR fluorescence of the GS-AuNPs and GS-AgNPs, we firstly performed noninvasively fluorescence imaging of the mice with injected nanoparticle to monitor their accumulations in submandibular salivary glands. GS-AuNPs and GS-AgNPs were intravenously injected to two groups of BALB/c mice (n=3) and then whole-body fluorescence images were obtained using in vivo imaging system (Woodbridge, CT) at 1, 3, 12- and 24-hours post injection (p.i.). As shown in Figure 2a, fluorescence signal in submandibular salivary glands (as indicated by the white circle) from the mice injected with GS-AgNPs can be observed after 1 h p.i. and reached the maximum value ~ 3 h p.i., followed by a decrease in intensity over time but a weak signal was retained in the region for more than 24 h. In contrast, the fluorescence signal of GS-AuNPs was significantly lower in intensity and was comparable to background signal across the imaging window (Figure 2b). It should be noted that the fluorescence signal observed from the abdominal area originated from the fluorescence of food in the intestine and stomach (Figure S2). The time fluorescence intensity curves of the submandibular salivary glands were obtained through quantitative analysis of whole-body images (Figure 2c), suggesting that GS-AgNPs exhibited a much more efficient accumulation in SSG than GS-AuNPs especially at the early transport stage. To further prove the location of the targeting site and the accumulation of NPs, the mice injected with GS-AgNPs were sacrificed and the SSG was collected and invasively imaged at 3h p.i.. The SSG exhibited strong fluorescence, confirming significantly high accumulation of GS-AgNPs in this organ (Figure 2d). The collected tissue was further verified to be SSG through histological study as discussed in the following section.

To gain more insight into the differences in accumulation of these two NPs to SSG, we intravenously injected both NPs into two groups of BLAB/c mice (n=3) and then sacrificed at 5 min, 3 and 24 h p.i., respectively. The organs of interest (SSG, blood, heart, lung, liver, spleen, kidney, stomach, muscle, skin, bone, membrane, intestine, and brain) were harvested and the amounts of NPs in these organs were accurately quantified using inductively coupled

plasma mass spectrometry (ICP-MS) (Figure S3–5). Accumulations of Au and Ag NPs in SSG at various time points p.i. have been shown in Figure 3a. Amount of GS-AuNPs in SSG was decreasing over time, whereas GS-AgNPs exhibited a significantly high accumulation at 3h p.i., ~ 6 times higher than that of GS-AuNPs, followed by 1.64%ID/g GS- AgNPs being cleared out of SSG from 3h p.i. to 24h p.i.. The results were consistent with the imaging studies described in Figure 2. To further unravel the nano-bio interactions of the NPs in main organs, especially in SSG, organ permeability for NPs (defined as organs-to- blood ratio at 5 min p.i.) and retention (defined as the ratio of 24 h / 5 min accumulation in each organs) were calculated, respectively. As shown in Figure 3b, GS-AgNPs exhibited ~ 8.6 times higher permeability (34.39% ± 7.13%) in SSG than that of GS-AuNPs (3.98% ± 1.12%) and such higher permeability can also be observed in other organs, suggesting an overall higher vascular permeability of GS-AgNPs in the whole body. The higher permeability of GS-AgNPs over GS-AuNPs was further confirmed by comparing their pharmacokinetics profiles, where GS-AgNPs showed significantly higher volume of distribution (V_d) than that of GS-AuNPs (8.97 ± 0.07ml, AgNPs vs 2.98 ± 0.08ml, AuNPs) (Figure 3C), suggesting that GS-AgNPs can more easily distribute to organs and background tissues than GS-AuNPs.[16] We also conducted blood vessel imaging of GS-AgNPs and GS-AuNPs in the mouse ear after iv injection of these two types of NPs to further evaluate their vascular permeability. As shown in the Figure S6, the fluorescence intensity of background tissue in GS-AgNPs group increased faster than that of the GS-AuNPs group. At 8min post injection, the blood vessel can still be clearly observed in GS-AuNPs group, but the blood vessels in the GS-AgNPs group were barely observed due to their rapid distribution in the background tissue, further indicating the higher permeability of GS-AgNPs than that of GS-AuNPs.

However, despite the fact that GS-AgNPs is more permeable than GS-AuNPs, its permeability to SSG is still lower than to other organs. Among all collected organs, apart from brain (which is hard to target due to the presence of blood-brain-barrier), SSG still exhibited least permeable to the both NPs among any other organs, consistent with previous finding that the low permeability of SSG is due to tight junctions between salivary gland epithelium.[17] Interestingly, despite of the low permeability, SSG is the organ that possessed the longest NPs retention regardless of the type of NPs (Figure 3d). Meanwhile, GS-AgNPs also exhibited longer retention in SSG compared to that of GS-AuNPs.

To gain more insight into the high accumulation and retention of GS-AgNPs in SSG, we conducted histological studies on the distribution of both NPs in SSG 3 h p.i.. The intra-salivary gland distribution of both NPs was investigated through histological studies. Tissue slides of SSG injected with GS-AgNPs and GS-AuNPs were prepared, respectively. Hematoxylin and eosin (H&E) stain was performed to visualize the physiological structures of SSG and silver stain was carried out to visualize the NPs. As shown in Figure 4a, GS-AgNPs were massively taken up by the striated duct (SD) cells (Figure 4c) and excretory duct (ED) cells (Figure 4e), whereas much fewer GS-AuNPs were found in these two duct cells (Figure 4b, 4d and 4f), suggesting that cellular uptake of GS-AgNPs by striated and excretory duct cells is much more efficient than that of GS-AuNPs. Meanwhile, neither GS-AgNPs nor GS-AuNPs could be found in acinar cell and intercalated duct cells (Figure 4c and 4d), which is due to the fact that both acinar cells and intercalated duct cells are covered by myoepithelial cells with tight junctions.[18] The tight junctions between myoepithelial

cells blocked the access of both GS- AuNPs and GS-AgNPs to acinar cells and intercalated duct cells (Scheme 1). More importantly, as shown in Figure 4e, GS-AgNPs can be released into the duct lumen (as indicated by the yellow circle) and finally drained into oral cavity with saliva, which could explain the decrease of GS-AgNPs in SSG from 3 h p.i. to 24h p.i. (Figure 3a).

In summary, we discovered a very interesting transport and clearance pathway of renal clearable AgNPs, which can selectively accumulate in SSG and be efficiently taken up by and excreted through the SSG. This is fundamentally due to the high vascular permeability of GS-AgNPs arising from its low material density. Moreover, GS-AgNPs can be efficiently excreted out of SSG into saliva. These findings suggest that it is possible to develop highly vascular-permeable engineered nanoparticles to target and clear out of salivary glands. In addition, since engineered nanoparticles, in particular, silver nanoparticles including GS-AgNPs[19] or GS-Ag_2S nanoclusters[20], have demonstrated broad-spectrum antibacterial and antiviral activities[21] and they are stable in saliva[22], it would be highly desired to further investigate these therapeutic functions in salivary glands in vivo and explore the feasibility of deactivating infectious bacteria and viruses in the saliva droplets in oral cavities to prevent disease transmission. This new transport route and nano-bio interaction of engineered nanoparticles potentially further broaden the application of nanomedicines in the fight against the infectious diseases such as COVID-19 pandemics.

Supplementary Material

Refer to Web version on PubMed Central for supplementary material.

ACKNOWLEDGMENT

The authors' work was supported by the NIH (1R01DK103363), Welch Research Foundation (AT-1974-20180324) and Cecil H. and Ida Green Professorship in Systems Biology Science of J.Z. from the University of Texas at Dallas.

REFERENCES

[1]. Hunter L, British Dental Journal 2013, 214, 425–425.

[2]. Nanci A. a., Ten Cate's oral histology : development, structure, and function, 9th edition. ed., Elsevier, St. Louis, Missouri :, 2018.

[3]. Treuting PM, Dintzis SM, in Comparative Anatomy and Histology (Eds.: Treuting PM, Dintzis SM), Academic Press, San Diego, 2012, pp. 111–120.

[4] a). Carpenter GH, Annu Rev Food Sci Technol 2013, 4, 267–276 [PubMed: 23464573] b)de Almeida Pdel V, Gregio AM, Machado MA, de Lima AA, Azevedo LR, J Contemp Dent Pract 2008, 9, 72–80. [PubMed: 18335122]

[5] a). Fábián TK, Hermann P, Beck A, Fejérdy P, Fábián G, Int J Mol Sci 2012, 13, 4295–4320 [PubMed: 22605979] b)Humphrey SP, Williamson RT, J. Prosthet. Dent 2001, 85, 162–169. [PubMed: 11208206]

[6] a). Brook I, Oral and Maxillofacial Surgery Clinics of North America 2009, 21, 269–+ [PubMed: 19608044] b)Lejal E, Moutailler S, Simo L, Vayssier-Taussat M, Pollet T, Parasites & Vectors 2019, 12c)Fekadu M, Shaddock JH, Baer GM, Journal of Infectious Diseases 1982, 145, 715–719d)Arrieta JJ, Rodriguez-Inigo E, Ortiz-Movilla N, Bartolome J, Pardo M, Manzarbeitia F, Oliva H, Macias DM, Carreno V, American Journal of Pathology 2001, 158, 259264e)Toussirot E, Le Huede G, Mougin CI, Balblanc JC, Bettinger D, Wendling D, Journal of Rheumatology

2002, 29, 2382–2385fXu RS, Cui BM, Duan XB, Zhang P, Zhou XD, Yuan Q, International Journal of Oral Science 2020, 12.

[7]. Li YQ, Ren B, Peng X, Hu T, Li JY, Gong T, Tang BY, Xu X, Zhou XD, Molecular Oral Microbiology.

[8]. Wang L, Hu C, Shao L, International journal of nanomedicine 2017, 12, 1227–1249. [PubMed: 28243086]

[9]. Yu M, Zheng J, ACS Nano 2015, 9, 6655–6674. [PubMed: 26149184]

[10] a). Choi HS, Liu W, Liu F, Nasr K, Misra P, Bawendi MG, Frangioni JV, Nat Nano 2010, 5, 42–47b)Burns AA, Vider J, Ow H, Herz E, Penate-Medina O, Baumgart M, Larson SM, Wiesner U, Bradbury M, Nano Letters 2009, 9, 442–448 [PubMed: 19099455] c)Zhou C, Long M, Qin Y, Sun X, Zheng J, Angew. Chem., Int. Ed 2011, 50, 31683172d)Liu J, Yu M, Ning X, Zhou C, Yang S, Zheng J, Angewandte Chemie International Edition 2013, 52, 12572–12576 [PubMed: 24123783] eTang S, Chen M, Zheng N, Small 2014, 10, 3139–3144. [PubMed: 24729448]

[11] a). Yu M, Zhou C, Liu L, Zhang S, Sun S, Hankins JD, Sun X, Zheng J, Angewandte Chemie International Edition 2017, 56, 4314–4319 [PubMed: 28295960] b)Liu J, Yu M, Zhou C, Zheng J, Materials Today 2013, 16, 477–486.

[12] a). Hyun H, Park MH, Owens EA, Wada H, Henary M, Handgraaf HJM, Vahrmeijer AL, Frangioni JV, Choi HS, Nat. Med 2015, 21, 192–197 [PubMed: 25559343] b)Hyun H, Wada H, Bao K, Gravier J, Yadav Y, Laramie M, Henary M, Frangioni JV, Choi HS, Angew. Chem., Int. Ed 2014, 53, 10668–10672.

[13]. Du B, Jiang X, Das A, Zhou Q, Yu M, Jin R, Zheng J, Nat Nanotechnol 2017, 12, 1096–1102. [PubMed: 28892099]

[14]. Tang S, Peng C, Xu J, Du B, Wang Q, Vinluan lii RD, Yu M, Kim MJ, Zheng J, Angewandte Chemie International Edition 2016, 55, 16039–16043. [PubMed: 27882633]

[15]. Zheng J, Zhou C, Yu M, Liu J, Nanoscale 2012, 4, 40734083.

[16]. Greenblatt DJ, Annu. Rev. Med 1985, 36, 421–427. [PubMed: 3994325]

[17]. Baker OJ, Tissue Barriers 2016, 4, e1162348. [PubMed: 27583188]

[18]. Redman RS, Microsc Res Tech 1994, 27, 25–45. [PubMed: 8155903]

[19] a). Taglietti A, Fernandez YAD, Amato E, Cucca L, Dacarro G, Grisoli P, Necchi V, Pallavicini P, Pasotti L, Patrini M, Langmuir 2012, 28, 8140–8148 [PubMed: 22546237] b)Yuan X, Setyawati MI, Tan AS, Ong CN, Leong DT, Xie JP, Npg Asia Materials 2013, 5.

[20]. Du T, Liang JG, Dong N, Lu J, Fu YY, Fang LR, Xiao SB, Han HY, Acs Applied Materials & Interfaces 2018, 10, 4369–4378. [PubMed: 29337529]

[21] a). Tang SH, Zheng J, Advanced Healthcare Materials 2018, 7b)Ngamchuea K, Batchelor-McAuley C, Compton RG, Nanotoxicology 2018, 12, 305–311. [PubMed: 29451053]

[22]. Lara HH, Garza-Trevino EN, Ixtepan-Turrent L, Singh DK, Journal of Nanobiotechnology 2011, 9.

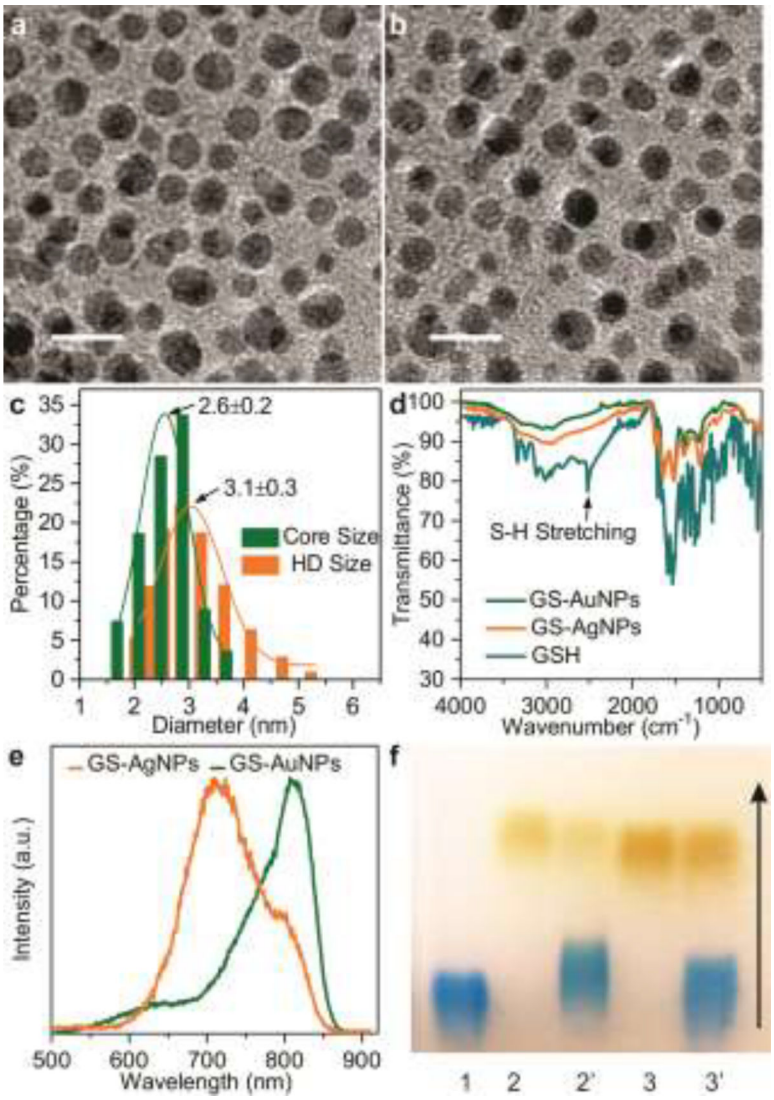

Figure 1.

Characterization of glutathione-coated Au and Ag nanoparticles. Typical transmission electron microscopy (TEM) image of GS-AuNPs (a) and GS-AgNPs (b). Scale bar=5 nm. (c) The GS-AgNPs have a core size of ~2.6 nm. Dynamic light scattering analysis gave HD= ~3.1nm in aqueous solution. (d) FTIR spectra of L- glutathione (GSH) reduced ligand, the Au and Ag NPs protected by the same ligand. The spectra show that the band around 2525 cm^{-1} disappears in the NPs spectra with respect to that of the ligand, indicating that the ligand is bound to the NPs via the sulfur atom. (e) Fluorescence emission spectra of GS-AgNPs and GS-AuNPs. (F) Agarose gel electrophoresis of the two kinds of NPs with or without incubation with fetal bovine serum (FBS). GS-AuNPs (well 2 and 2'), GS-AgNPs (well 3 and 3') were incubated in the absence (well 2, 3) or presence (well 2', 3') of 10% (v/v) CBB250-stained FBS at 37 ^{o}C for 30 min, indicating no obvious protein binding for both nanoparticles. Blue band in wells 1= CBB250-stained FBS proteins.

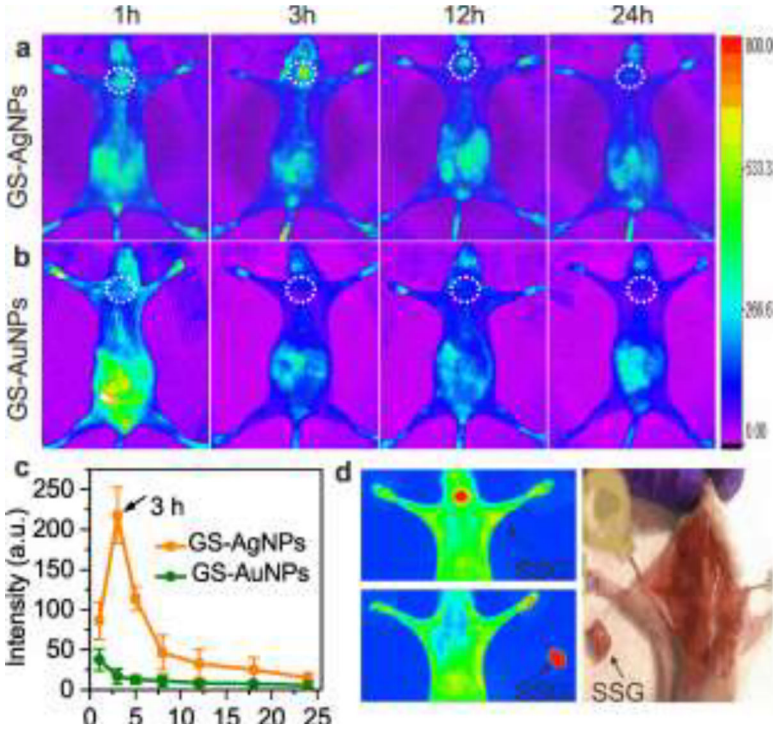

Figure 2.

Whole-body fluorescence images of mice i.v. injected with NPs. (a) GS-AgNPs showed more effective targeting to SSG (marked by a white circle) than GS-AuNPs (b). (c) The time fluorescence intensity curves of the submandibular salivary glands were obtained through quantitative analysis of whole-body fluorescence images. (d) High accumulation of GS-AgNPs in SSG was further confirmed by invasive and bright field imaging.

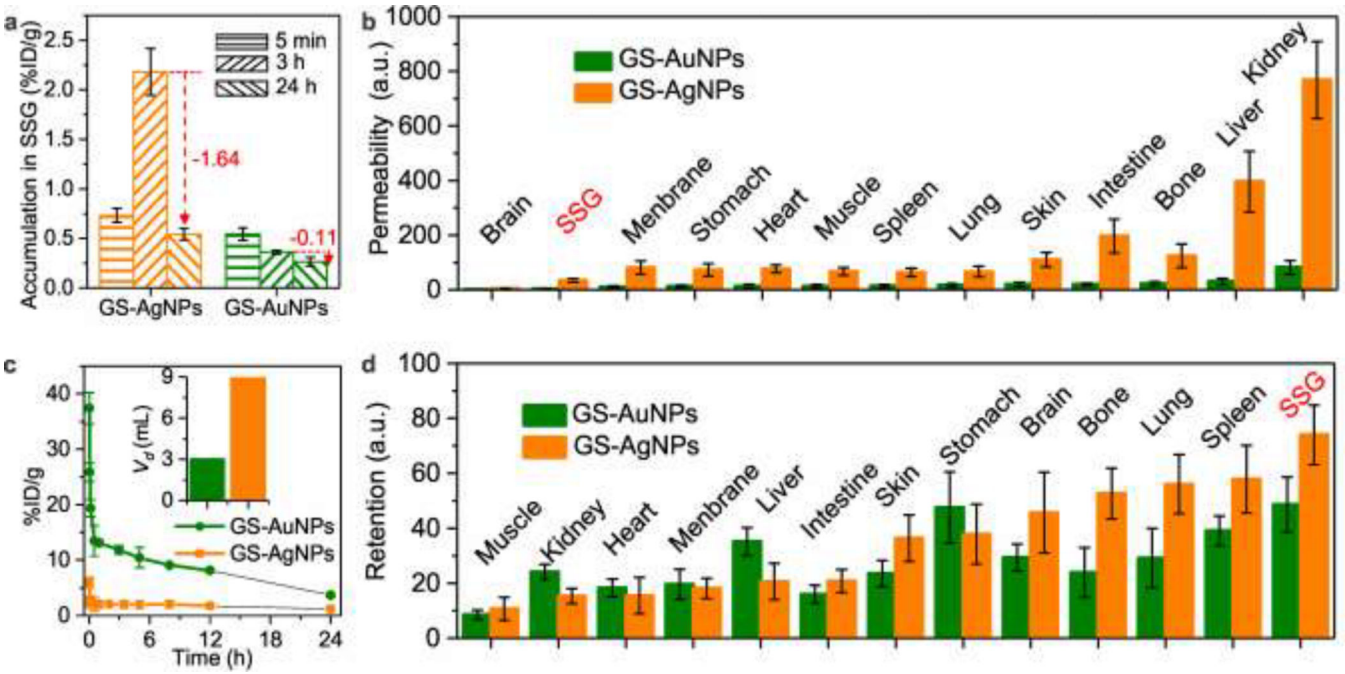

Figure 3.

Submandibular salivary glands (SSG) possessed the lowest permeability (except for brain) and highest NPs retention for the both NPs. (a) Accumulation of GS-AuNPs and GS-AgNPs in SSG at 5 mins 3 and 24 h p.i.. (b) NPs' permeabilities in various organs (defined as organs-to-blood ratio at 5 min p.i.). (c) Pharmacokinetics profiles and V_d (insert) of the both NPs. (D) Retentions of the two NPs (defined as the ratio of 24 h / 5 min accumulation in each organs).

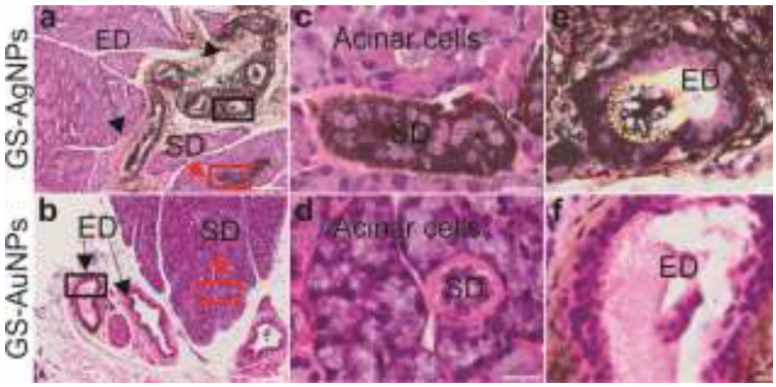

Figure 4.

Histological analysis of GS-AgNPs and GS-AuNPs distribution in different SSG compartments at 3h p.i. with H&E and silver enhancement staining. Arrows in red indicate striated duct (SD) and arrows in black indicate excretory duct (ED). (a) GS-AgNPs was massively uptaken by the SD cells and ED cells, and then released into duct lumen. Scale bar, 100 μm. (c) Represented a high magnification of SD (the red squared area in "a"). Scale bar, 20 μm. (e) Represented a high magnification of ED (the black squared area in "a") and released AgNPs can be found in lumen (marked by a yellow circle). Scale bar, 20 μm. (b) Much fewer GS-AuNPs was found inside these two duct cells. Scale bar, 100 μm. (d) Represented a high magnification of SD (the red squared area in "b"). Scale bar, 20 μm. (e) Represented a high magnification of ED (the black squared area in "b"). Scale bar, 20 μm.

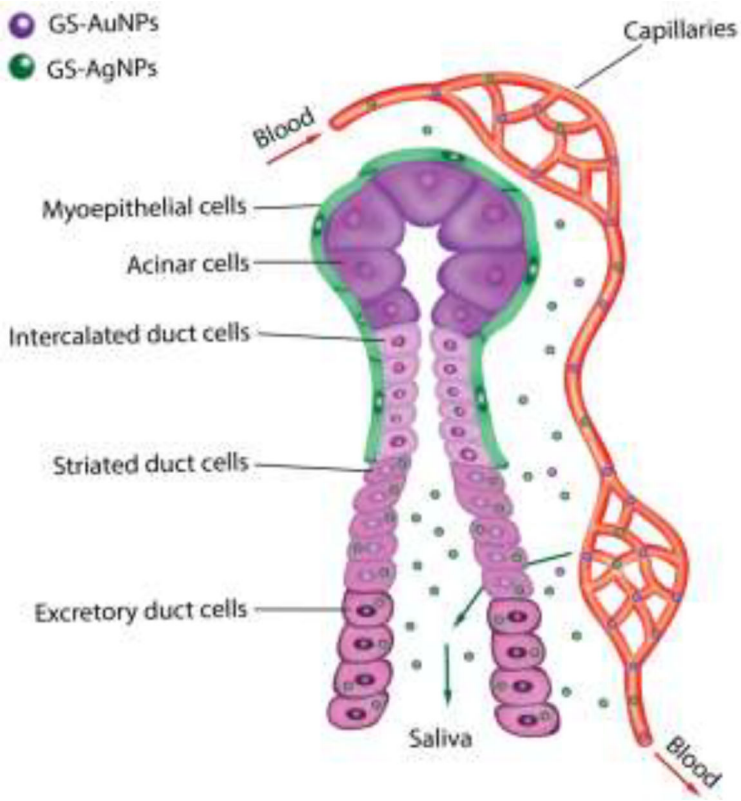

Scheme 1.

Mechanism scheme showing the permeability, retention and clearance of GS-AuNPs (brown) and GS-AgNPs (blue) in SSG. Compare with GS-AuNPs, due to the higher vascular permeability, GS-AgNPs can more easily extravasate from blood vessels into the SSG, be uptaken by striated and excretory duct cells and finally eliminated into saliva. Moreover, the uptake of NPs by acinar cells and intercalated duct cells is blocked due to the presence of myoepithelial cells with tight junctions.